# INSIGHTS ON THE INDIAN OCEAN TECTONICS AND GEOPHYSICS SUPPORTED BY GMT

*POLINA LEMENKOVA*[1]

**Abstract. Insights on the Indian Ocean Tectonics and Geophysics Supported by GMT.** This paper presented analyzed and summarized data on geological and geophysical settings about the tectonics and geological structure of the seafloor of the Indian Ocean by thematic visualization of the topographic, geophysical and geological data. The seafloor topography of the Indian Ocean is very complex which includes underwater hills, isolated mountains, underwater canyons, abyssal and accumulative plains, trenches. Complex geological settings explain seismic activity, repetitive earthquakes, and tsunami. Understanding and prognosis of the disastrous and catastrophic geological events is strongly based on correct data analysis, modelling and visualization. An important feature of this paper is mapping multi-source high-resolution data by GMT. Data include raster grids in NetCDF and GRD formats: ETOPO1, geologic and m*arine free-air gravity* data, *EGM96, age, spreading rates, and spreading asymmetry of the ocean crust by NOAA, total sediment thickness. Data were visualized by GMT modules to compare and analyze geophysical and geological settings of the Indian Ocean. Visualization reveled correlations between high bathymetric variations of the oceanic seafloor, distribution of main geological seafloor fabric: Southwest, Southeast, Mid and Carlsberg ridges. Tectonic maps were plotted to perform comparative analysis of several variables: crust age, spreading half rates (mm/yr), asymmetries in crustal accretion on conjugate ridge flanks (%), variations in the geopotential and gravimetric models. Being the warmest of the world's ocean, Indian Ocean has specific climatic conditions (repetitive monsoons, tsunamis, cyclones and storms), complex geologic seafloor structure with triple junction and unique geographic settings. Presented paper contribut ed to the regional studies of the Indian Ocean.*

**Keywords**: Indian Ocean, geomorphology, seafloor, geophysics, topography, GMT

## 1. INTRODUCTION

This study is focused on the Indian Ocean by means of the thematic visualization of the topographic, geophysical and geological raster grids using Generic Mapping Tools (GMT). The Indian Ocean is the 3rd largest ocean (70,56 million km$^2$) after Pacific and Atlantic. The seafloor topography of the Indian Ocean is very complex. It includes underwater hills, separate isolated mountains, abyssal plains, accumulative plains, two deep-sea trenches.

1 Schmidt Institute of Physics of the Earth, Russian Academy of Sciences Laboratory of Regional Geophysics and Natural Disasters (No. 303). 10 Bolshaya Gruzinskaya St., Bld. 1, Moscow, 123995, Russian Federation. Tel.: +007-916-298-37-19. pauline.lemenkova@gmail.com https://orcid.org/0000-0002-5759-1089

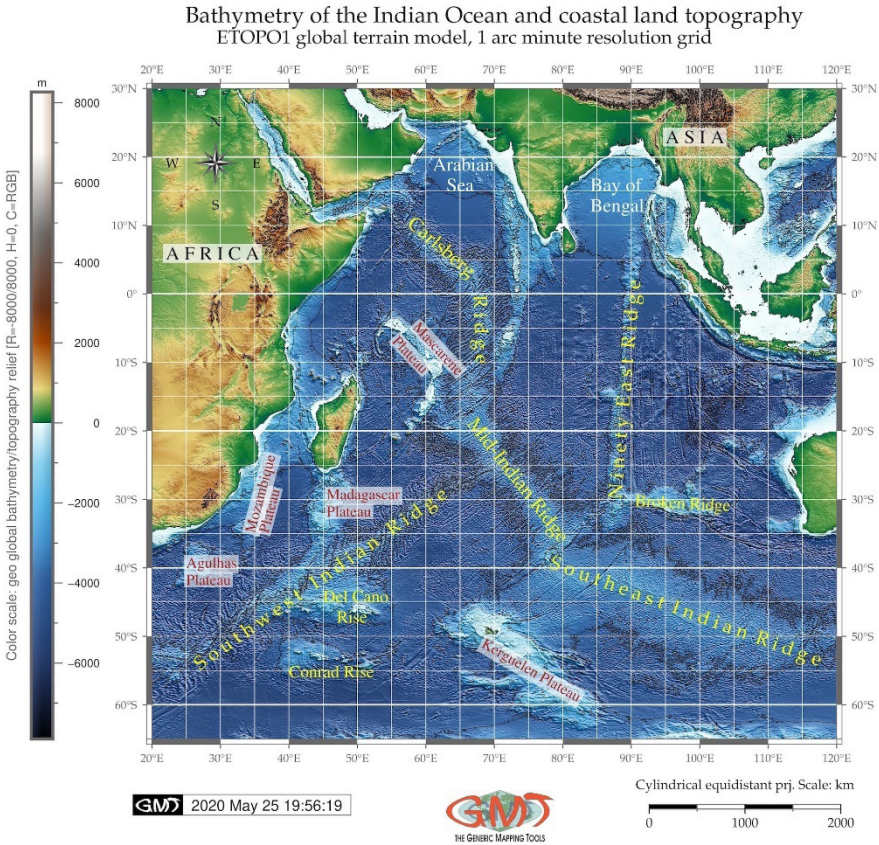


**Fig. 1.** Topographic map of the study area: Indian Ocean. Mapping: GMT. Source: author.

Underwater canyons on the continental slopes and semi-suspended turbidity currents flows contribute to the formation of the Indian Ocean seafloor (Udintsev, 1959). The area of the Indian Ocean is ca. 2.3 times less than the area of the Pacific Ocean (161,76 M km$^2$) and one quarter less than Atlantic (85,13 M km$^2$), but ca. 5 times more the area of the Arctic Ocean (15,56 M km$^2$). Three ridges form a single system of the Mid-Indian Ridge at Arabia–India–Somalia triple junction (a.k.a. Aden–Owen–Carlsberg) with Carlsberg and Southeast Indian ridges (Figure 1). Indian Ocean bathymetry has isometric outlines and vertically extended geometry with greatest width from westward ca. 8000 km, and southward – 9656 km. Average depth of the Indian Ocean is 3741 m and extreme depth is 7906 m (Eakins & Sharman, 2010). Between the southern outskirts of Africa and Australia on one side and the northern edge of Antarctica, on the other, there are wide and deep passages (1930-2500 km width, 4-5 km depth) through which

water masses of the Indian Ocean mix with Pacific and Atlantic oceans enabling global circulation (Figure 1). The area of shelf with depths lesser than 200 m takes only 6.1% of the total area, which is larger than in the Pacific Ocean (4.6%), but lesser than in the Atlantic (8.6%), and much lesser (39.6%) than in the Arctic Ocean *(Leontiev & Udintseva, 1971)*.

## 2. MATERIALS AND METHODS

Data include several raster grids taken from the public sources of NOAA:

1. ETOPO1 1 arc-minute global relief model of Earth's surface that integrates land topography and ocean bathymetry by NOAA (Amante & Eakins, 2009) in GRD format.
2. Geologic layers of Scripps Institution of Oceanography and School of Ocean and Earth Science and Technology, University of Hawaii, U. S.: faults, trenches, ridges, fracture zones (Wessel & Smith, 2018; Matthews et al. 2011; Seton et al. 2014) in native vector GMT format (e.g. trench.gmt).
3. Marine free-air gravity data based on remote sensing data from Geosat, ERS-1 altimetry, CryoSat-2 and Jason-1, ESA (Smith & Sandwell, 1995; Sandwell et al. 2014) in GRD format.
4. Geoid based on the Geopotential Model EGM96 in GRD format (Lemoine et al. 1998).
5. Age, spreading rates, and spreading asymmetry of the world's ocean crust raster NetCDF grids by NOAA (Muller2008). The age units are in millions of years times 100. The area was selected from the global geographic grid, 2 arc min resolution, gridline-registered. The metadata were checked up by GDAL library (GDAL/OGR contributors, 2020).
6. Total Sediment Thickness of the World's Oceans and Marginal Seas Version 3 (GlobSed) 5 arc minute resolution grid by NOAA, NetCDF format (Straume et al. 2019).
7. Color palettes from GMT and external sources (Crameri, 2018; Crameri & Shephard, 2019).

The GMT cartographic scripting toolset was selected as a main software for plotting maps (*Wessel et al. 2013; Wessel et al. 2019)*.

In contrast with tradition GIS, e.g. ArcGIS (*Gauger et al. 2007; Lemenkova, 2011; Suetova et al. 2005a; 2005b; Klaučo et al. 2013a; 2013b; 2014; 2017; Kuhn et al. 2006)*, the approach of GMT consists in console-based shell scripting where all cartographic elements (legend, grid, projections, colors, title, fonts, vector and raster layers) are being plotted from the command line using available techniques described previously (Lemenkova, 2020a; 2020b; 2019a; 2019b; 2019c, 2019d).

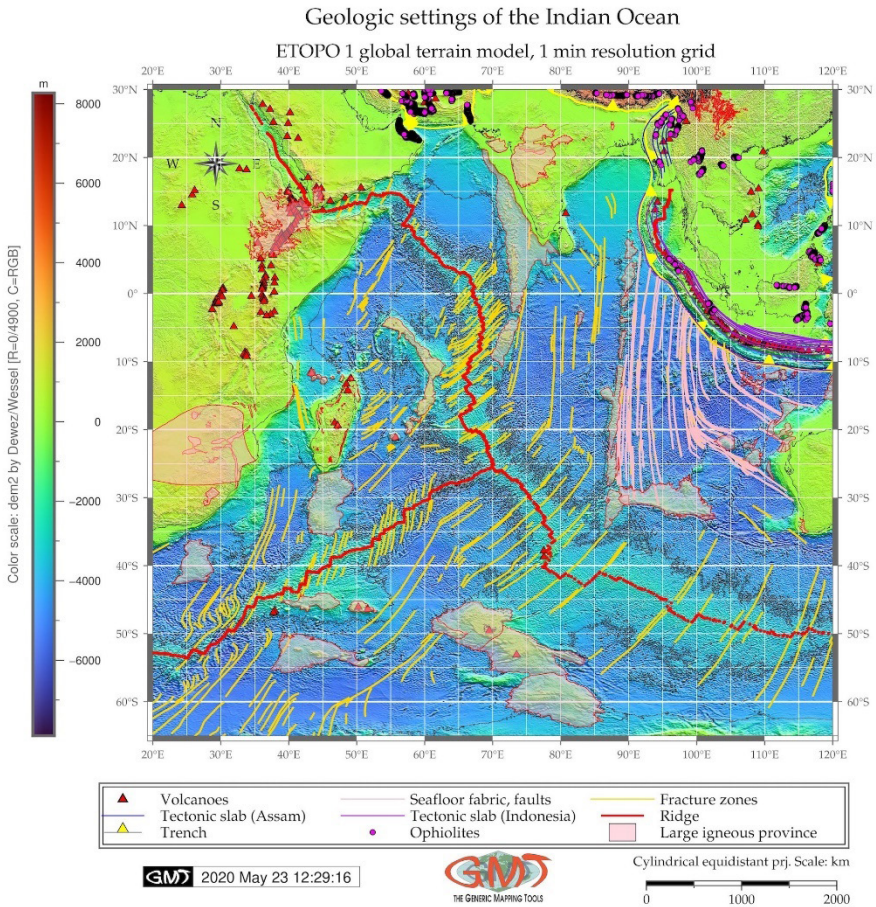


**Fig. 2.** Geological settings in Indian Ocean region. Mapping: GMT. Source: author.

Using command line programming in cartographic routine significantly advances working routine, since it enables reprocessing the data using scripts through technical repeatability of scripts, decreases time of data processing and precision of machine learning based approach, as already been demonstrated in works on automatization and machine learning in GIS (*Schenke & Lemenkova, 2008;* Lemenkova, 2019e; 2019f; 2019g; *Lemenkova 2018*). All presented maps were visualized in GMT.

## 3. TOPOGRAPHY

Topographic variations in the Indian Ocean are significant comparing to other oceans. The depth range from 200–4000 m, typical for the continental slope is significant with 42% (compare with Pacific Ocean: only 35.6%) approaching the area occupied by seabed basins (4000–6000 m), 51% (Pacific Ocean: 58.1%, Atlantic: 49.1%).

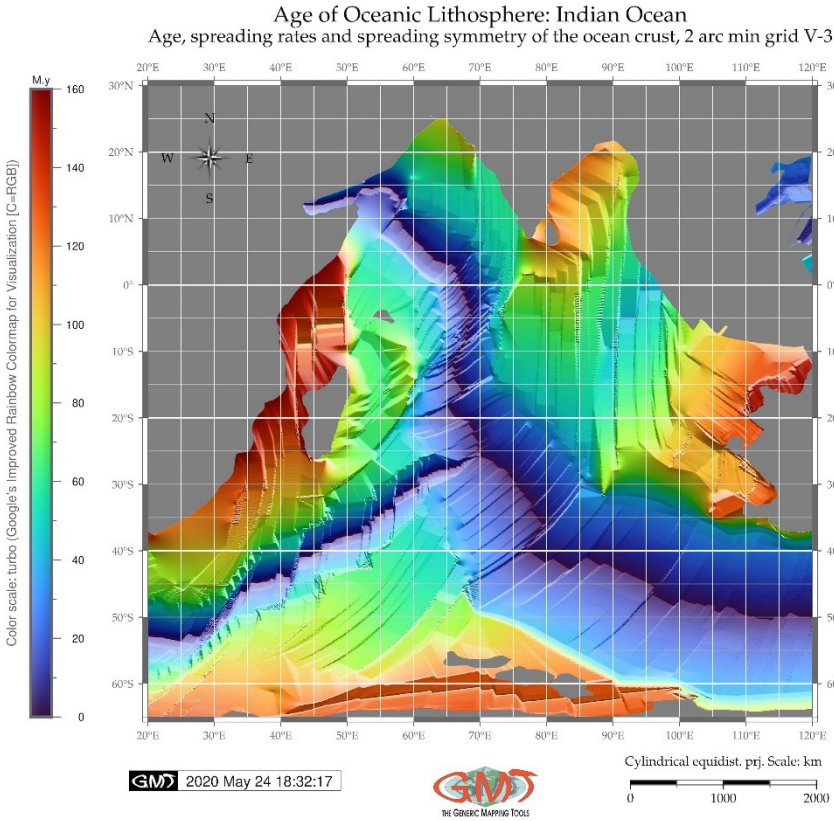


**Fig. 3.** Age of oceanic lithosphere: Indian Ocean. Mapping: GMT. Source: author.

Depths >6000 m, typical for the deep-sea trenches are rare (0.8%). The region of depths of 200-4000 m in the Indian Ocean is morphologically more heterogeneous than in the Atlantic and Pacific oceans. In Indian Ocean it is almost equally divided between the mid-ocean ridges, hills and ridges of the seabed and continental slope, while in the Atlantic and Pacific oceans, most of the such depths is taken by mid-ocean ridges.

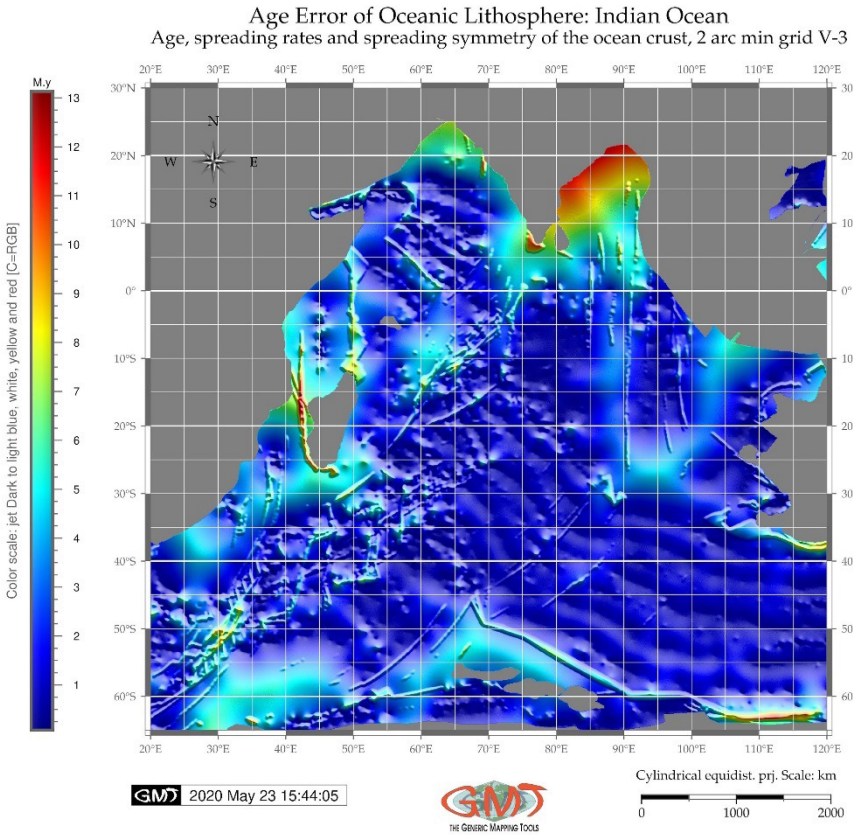


**Fig. 4.** Age error of oceanic lithosphere: Indian Ocean. Mapping: GMT. Source: author.

A specific feature of the submarine relief of the Indian Ocean basin consists in its numerous ridges and elevations, classified as aseismic uplifts, and marginal plateaus of the continental margins. Neither the Atlantic nor the Pacific have such numerous uplifts and plateaus comparing to other geomorphic structures. The aseismic uplifts differ from seismically active mid-ocean ridges in their axial parts. Large aseismic ridges of the Indian Ocean lie in its western sector: the Mascarene Plateau with the Seychelles and Madagascar. Significantly smaller are the Owen Fracture Zone and Davie Fracture Zone, a submarine extension of the East African Rift (*Udintsev, 1989*). The Mozambique Ridge is formed by the geomorphic extension of the continental margin. A large submarine Agulhas Plateau is separated from the continent. Thus, the western sector of the Indian Ocean is subdivided into separate basins by the uplifts and ridges: Somali, Madagascar, Mozambique, Transkei and Agulhas basins (Figure 1).

## 4. GEOMORPHIC SCHEME OF THE INDIAN OCEAN BASIN

The most remarkable geologic feature of the Indian Ocean geomorphology is its active three spreading ridges dividing it into 3 sectors as 3-branched system of the mid-ocean ridge: Western, North-Eastern, Southern, meeting at the Rodrigues Triple Point (Figure 2, red line).

These ridges include the followings:

1. Central Indian Ridge is directed northward and then turns to the northwest entering the Gulf of Aden. This branch is separating the African from the Indian Plate.
2. Southwest Indian Ridge. The 2nd branch goes southwest in a westward direction, entering the Atlantic Ocean where it it connects with the Mid-Atlantic Range separating the African from the Antarctic Plate;
3. Southeast Indian Ridge is the 3rd branch which is directed in southeast, gently turning to the east, and then sharply shifts southwards at the entrance to the Pacific Ocean between Tasmania and Antarctica where it connects to the mid-ocean ridge of the Pacific Ocean separating the Australian from the Antarctic Plate.

The connection node between these three branches lies in the center of the Indian Ocean (Figure 2). As a consequence, three branches of the Mid-Indian Ridge separate the Indian Ocean into 3 sectors which include the underwater margins of the continents and seabed, divided into isolated basins by uplifts and local ridges.

Such complex and specific structure causes variations in the seafloor geomorphology of the Indian Ocean basin and briefly illustrates deep geologic inter-connection of the morphology between the Pacific, Atlantic and Indian Ocean.

## 5. SEAFLOOR TECTONICS OF THE INDIAN OCEAN

As can be seen (Figure 3), the age of the oceanic lithosphere in Indian Ocean is the youngest in the areas of Mid-Ocean Ridge (dark-blue to black areas, <20 M years) and the oldest date (120-160 M years, red colors on Figure 3) for the shelf areas near African coast (eastern area), Bay of Bengal and the Antarctic.

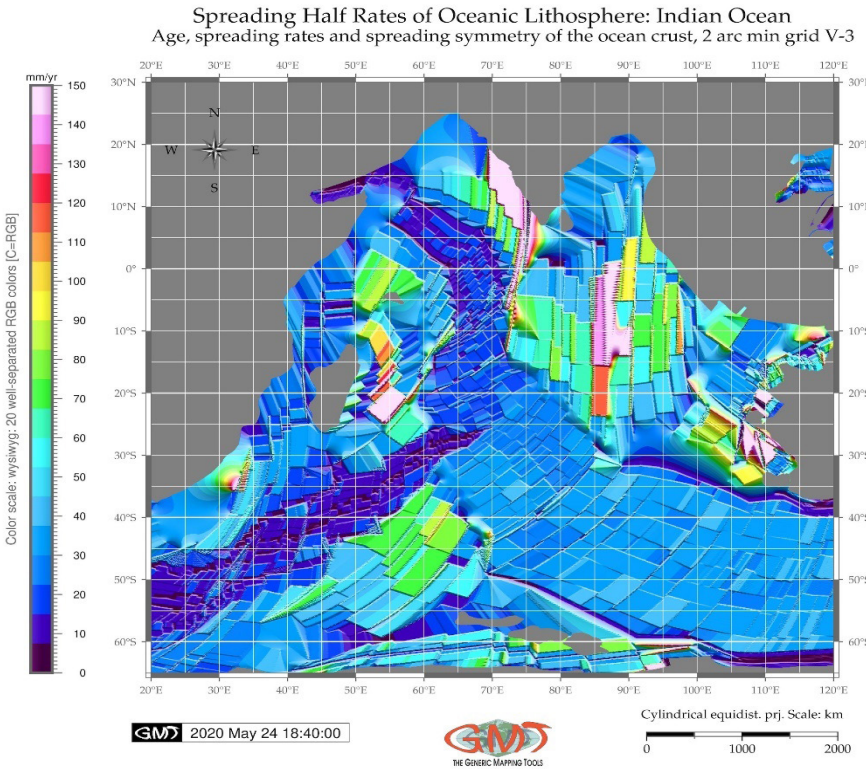


**Fig. 5.** Spreading half rates of lithosphere: Indian Ocean. Mapping: GMT. Source: author.

The rest of the areas is covered by the crust of various ages (e.g. 60-90 M years, green colors, 90-110 M years, yellow to orange, Figure 3). This corresponds to the studies on the tectonic history of the Indian Ocean which opened since Mesozoic (156 Ma) with African separation from East Gondwana and separated from Australia-Antarctica around 135–125 Ma, in Cretaceous (Chatterjee et al. 2013). The opening of the western part of Indian Ocean started in Late Cretaceous, followed by rapid movement of the Indian Plate to the northeastward to its present position, although before that it was moving to the north-west (*Kanaev, 1979*).

Such changes in tectonic movements were caused by the restructuring of the rift zones and the formation of the new axes of the mid-ocean ridge extension (*Hain, 1979*). Age errors may arise due to the mathematical approximations in the original model, therefore, age error grid gives information about the crustal age uncertainty (Figure 4). The highest uncertainty is notable for the oldest areas located in the Bay of Bengal (10–13 M yrs), red colors on Figure 4. The majority of the Indian Ocean basin do not exceed 5 M years (blue areas, Figure 4).

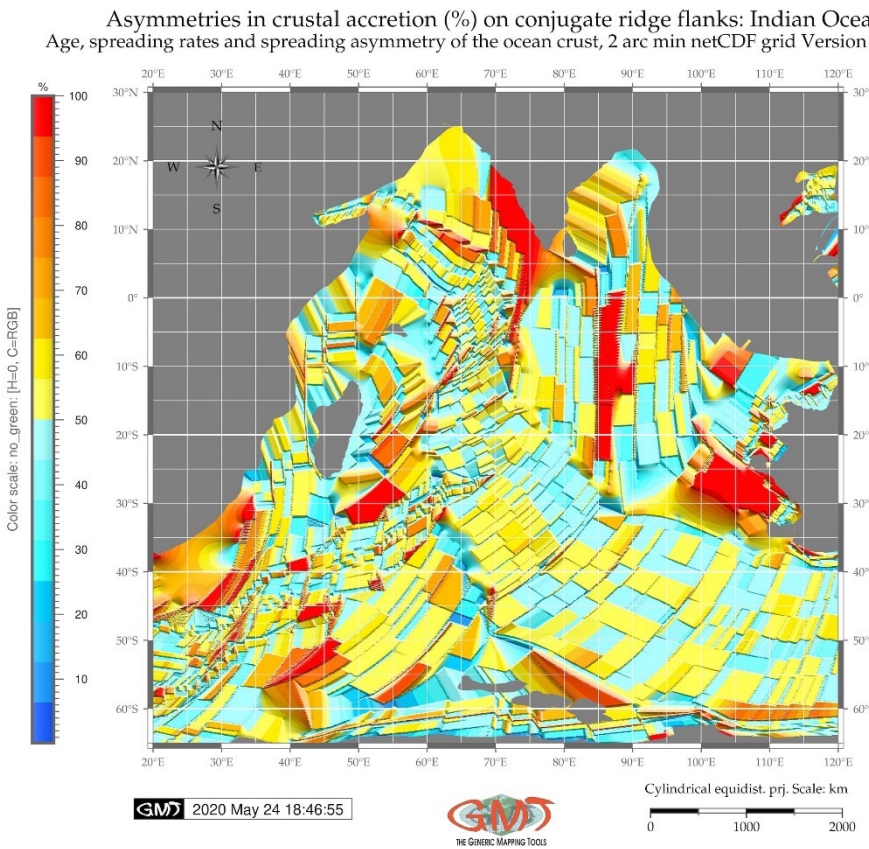


**Fig. 6.** Asymmetry in crustal accretion of the oceanic lithosphere: Indian Ocean. Mapping: GMT. Source: author.

The general concept of the spreading rates reflects the geological process of the mid-ocean ridge formation, when new oceanic crust is formed through volcanic activity and gradually moves away from the ridge (*Macdonald, 1982; 2019*). Because the movement of the oceanic lithosphere goes on both sides from the ridge, a concept of half spreading rate is introduced. Thus, spreading half rates is indicated by the rate of adding new oceanic lithosphere to each tectonic plate on either side of a mid-ocean ridge. Thus, it indicates a rate at which the Indian Ocean basin widens due to seafloor spreading with rough division to fast (>90 mm/yr), intermediate (40–90 mm/yr) and slow (<40 mm/yr). As can be seen (Figure 5), the opening for the Indian Ocean is the fastest in the Bay of Bengal (130-150 mm/yr, pink colors), followed by 105-128 mm/yrs (orange to red colors, southern Bengal).

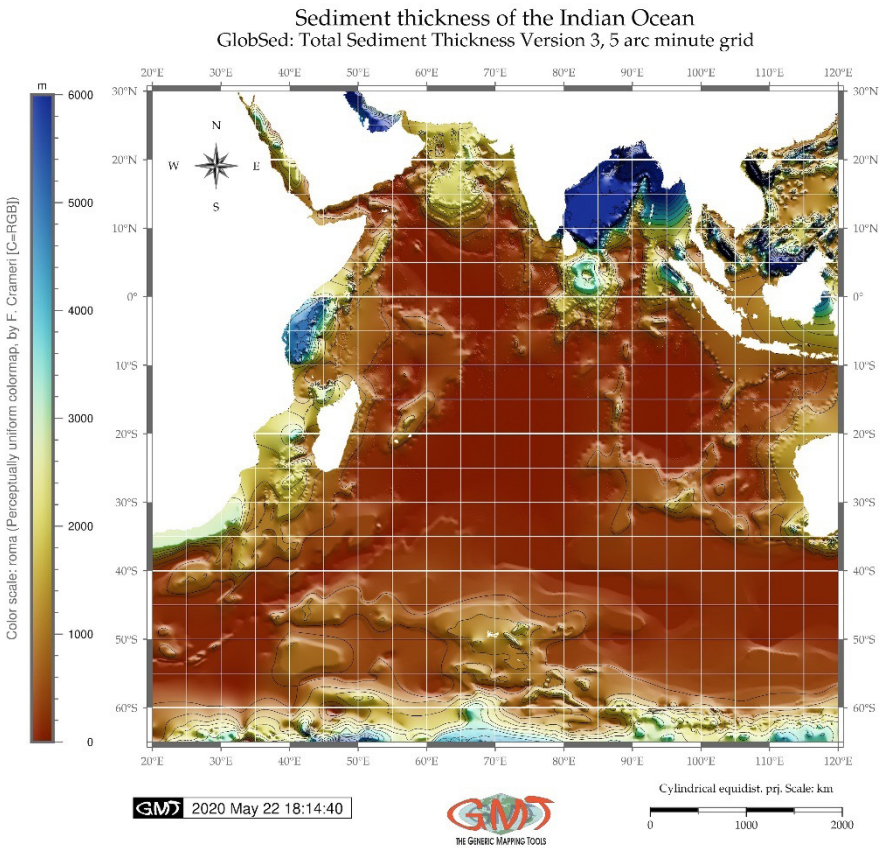


**Fig. 7.** Sediment thickness: Indian Ocean. Mapping: GMT. Source: author.

Intermediate speed values are 70-90 mm/yrs (green colors, south-west Indian Ocean). However, the majority of the spreading rates have rather low values for the Indian Ocean: 15-45 mm/yrs (blue colors, Figure 5). In Indian Ocean the subduction increases from the continental margins to pre-continental troughs, reaching 4–7 km, and over 8 km in the Sunda deep-sea trench. Because the age of the formation of the continental margins coincides with the start of Gondwana's movements in the Indian Ocean (ca. 160 M), the subduction rate in the Late Mesozoic and Cenozoic was lower. However, during geologic development, the speeds of vertical movements could changed significantly, speeding up or slowing down which is reflected in the variations in the spreading half rates (Figure 5). However, the general tendency toward subduction resulted in the formation of the epicontinental platforms.

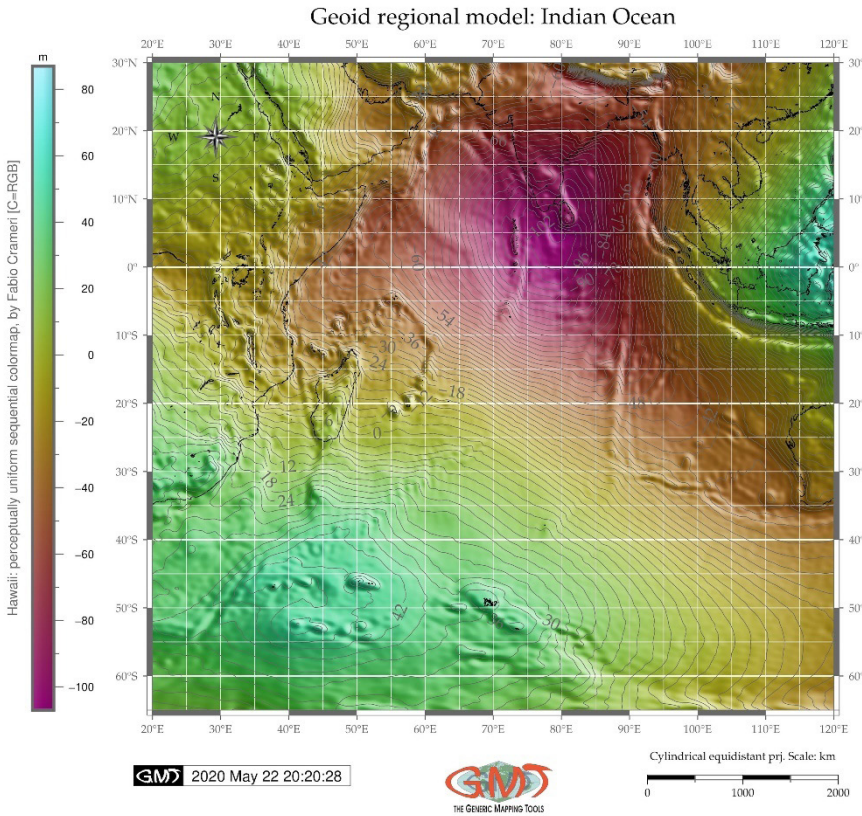


**Fig. 8.** Geoid model (EGM96): Indian Ocean. Mapping: GMT. Source: author.

The phenomena of the asymmetry in seafloor crustal accretion is caused by the complexity of geological processes causing significant variations along and across ridge segments: magnetization, hydrothermal factors, tectonic strain, mantle thermal structure, magma localization and detachment across the mid-ocean ridge axis (*Paulatto et al. 2015; Weissel & Hayes 1971; Müller et al. 2008*). Asymmetry in crustal accretion of the Indian Ocean (Figure 6) shows following findings. Crustal accretion percentage on conjugate ridge flanks (%) to be the highest (80-100%) for the areas eastern part of the Arabian Sea, south-east of Madagascar and west Australian coast. On the contrary, the lowest values of 20-62% (Figure 6) are dominating for the Indian Ocean and some fragmentary spots have values above 62% to 80% (orange colored areas, Figure 6).

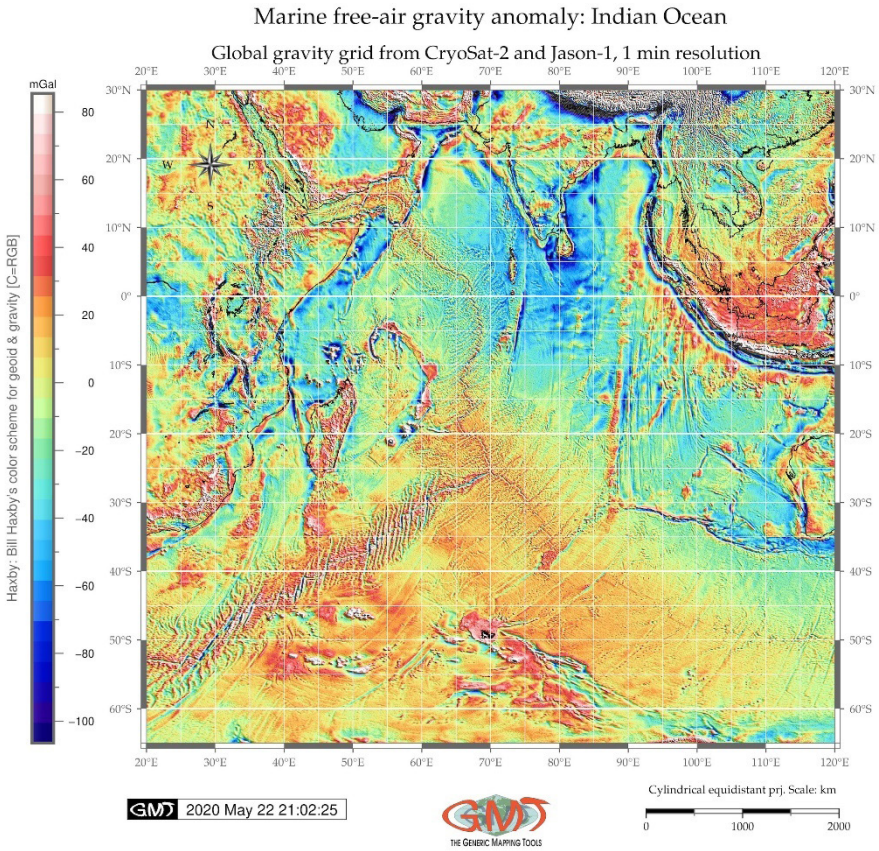


**Fig. 9.** Marine free-air gravity map: Indian Ocean. Mapping: GMT. Source: author.

## 6. SEDIMENTATION AND GEOLOGY

The sedimentary cover over the Indian Ocean covering the unevenness of the basement surface is distributed according to the geomorphological landforms and closeness to the major rivers, mostly the Bay of Bengal with discharging Ganges river which results in high values of sediment thickness in this area up to 5000-6000 m (Figure 7, dark blue colors). The sedimentary cover on the Mid-Ocean Ridges of the Indian Ocean has values of 500-1000 m (brown colors, Figure 7). As reported in previous studies (*Litvin 1987*) it has a nesting distribution and is distinguished by acoustic transparency. In the rift zone, the sedimentation is practically absent or their thickness is insignificant (values below 500 m, dark brown colors on Figure 7), with the exception of the deepest sections of the transverse troughs. The sediment thickness of precipitation increases to 1500-2000 km on the Kerguelen Plateau and Del Cano Rise (beige colors, Figure 7).

A continuous cover of sediments is widespread in the southern part of the West Indian Ridge. In other areas of the Mid-Ocean Ridge such sedimentary cover appears only at the outer boundaries of the ridge. The smallest precipitation thickness (about 0.1 km) is observed in the Central Massif and western Australian-Antarctic Rise.

## 7. GEOPHYSICAL MODELS OF THE INDIAN OCEAN BASIN

There are some variations in the geoid undulation values over the basin of the Indian Ocean with clear depression of India and adjacent Bay of Bengal and the Arabian Sea, 70-105 m. On the contrary, higher geopotential model values are notable over Conrad Rise and Del Cano Rise (Figure 8). Modelling marine free-air gravity over the Indian Ocean shows following results. The most areas of the basin are marked by weakly positive marine free-air gravity anomalies (0-20 mGal) on raised elevations and hills, 20–40 mGal above the elevations of the Agulhas Plateau, the ridges of Mozambique, Madagascar, Mascarene Plateau and the atolls of the Maldives, increase up to 50 mGal over shallow banks (Seychelles), but decrease to zero or negative values in the depressions, e.g. the Bay of Bengal (Figure 9).

Gravity anomalies are slightly higher (40 to 60 mGal) above the East Indian and West Australian ridges, and noticeably increase on the Kerguelen Plateau reaching 80 mGal, which is caused by the decreased bathymetric depths and increased crustal thickness (Figure 9). This corresponds to the previous studies on gravimetry of the Indian Ocean (*Gaynanov 1980*) reporting that Bouguer anomalies above the uplifts range from 240 to 160 mGal, and decrease to 80 mGal above the most elevated parts of the Kerguelen Plateau, Mascarene Plateau and the atolls of the Maldives. A complex interpretation of the gravimetric and seismic data models suggests possible presence anomalous upper mantle with a density reduced to 0.2 g / cm3 to depths of 25-30 km under the ridges of the East Indian and West Australian (*Udintsev 1989*).

## 8. CONCLUSION

The actuality of the presented study consists in a detailed description of the submarine relief of the Indian Ocean and interpreted information about geophysical fields and geological structure of its seafloor. The seafloor topography is one of the most important characteristics of the oceans. Ocean exploration always requires detailed and precise maps based on bathymetry, geological and geophysical data visualization. As important part of the ocean system, submarine relief significantly affects the dynamics of the water column and biological development of marine life. The particular importance has a seafloor topography which serves as a reflection of its deep geological structure.

Studies of the seafloor topography, geology and geophysical have always been and remain to be a matter of great practical importance due to the mineral exploration of the ocean resources. Together with data on the sediment structure, distribution of geophysical fields and composition of the basement rocks of the seafloor, seafloor topography presents the background for the studies of the marine geology and tectonics. Overlay of the multi-source data on morphological sculpture of the seafloor with data on the rocks structure and composition of the sedimentary cover provides a basis for further studies on reconstructions of the submarine relief formation and paleogeographic retrospective portrayal of the World Ocean. With application of the GMT for precise mapping of the seafloor topography and geology, this paper contributes to the regional studies of the Indian Ocean and presents usage of GMT for geographical data visualization.

**ACKNOWLEDGEMENTS**

This research was supported in the framework of the project No. 0144-2019-0011, Schmidt Institute of Physics of the Earth, Russian Academy of Sciences.

## REFERENCES

1. Amante C., Eakins B.W., (2009), *ETOPO1 Global Relief Model converted to PanMap layer format*. NOAA-National Geophysical Data Center, PANGAEA.
2. Chatterjee S., Goswami A., Scotese C.R. (2013), *The longest voyage: tectonic, magmatic, and paleoclimatic evolution of the Indian plate during its northward flight from Gondwana to Asia*. Gondwana Research. 23 (1): 238–267.
3. Crameri F., (2018), *Geodynamic diagnostics, scientific visualisation and StagLab 3.0*, Geoscientific Model Development, 11, 2541-2562.
4. Crameri F., Shephard, G. E. (2019), *Scientific Colour Maps*.
5. Eakins, B.W., Sharman G.F., (2010), *Volumes of the World's Oceans from ETOPO1*, NOAA National Geophysical Data Center, Boulder, CO.
6. Gaynanov A.G., (1980), *Gravimetric studies of the earth's crust of the oceans*. Moscow, MSU Press.
7. Gauger S., Kuhn G., Gohl K., Feigl T., Lemenkova P., Hillenbrand C., (2007), *Swath-bathymetric mapping*. Reports on Polar and Marine Research, 557, 38–45.
8. GDAL/OGR contributors, (2020), *GDAL/OGR Geospatial Data Abstraction software Library*, Open Source Geospatial Foundation
9. Hain V.E., (1979), *Regional Geotectonics*. Out-Alpine Asia and Australia. Moscow, Nedra. 356 p.
10. Kanaev V.F., (1979), *Relief of the bottom of the Indian Ocean*. Moscow, Nauka, 267 pp.
11. Klaučo M., Gregorová B., Stankov U., Marković V., Lemenkova P., (2013a), *Determination of ecological significance based on geostatistical assessment: a case study from the Slovak Natura 2000 protected area*. Central European Journal of Geosciences, 5(1), 28–42.

12. Klaučo, M., Gregorová, B., Stankov, U., Marković, V., Lemenkova, P. (2013b), *Interpretation of Landscape Values, Typology and Quality Using Methods of Spatial Metrics for Ecological Planning*. 54th International Conference Environmental & Climate Technologies, October 14, 2013, Riga, Latvia.
13. Klaučo, M., Gregorová, B., Stankov, U., Marković, V., Lemenkova, P. (2014), *Landscape metrics as indicator for ecological significance: assessment of Sitno Natura 2000 sites, Slovakia*. Ecology and Environmental Protection. Proceedings of the International Conference, March 19–20, 2014. Minsk, Belarus, 85–90.
14. Klaučo, M., Gregorová, B., Stankov, U., Marković, V., Lemenkova, P. (2017), *Land planning as a support for sustainable development based on tourism: A case study of Slovak Rural Region.* Environmental Engineering and Management Journal, 2(16), 449–458.
15. Kuhn G., Hass C., Kober M., Petitat M., Feigl T., Hillenbrand C.D., Kruger S., Forwick M., Gauger S., Lemenkova P., (2006), *The response of quaternary climatic cycles in the South-East Pacific: development of the opal belt and dynamics behavior of the West Antarctic ice sheet*. In: Gohl, K. (ed). Expeditionsprogramm Nr. 75 ANT XXIII/4, AWI. DOI: 10.13140/RG.2.2.11468.87687
16. Lemenkova P., (2020a), *GMT Based Comparative Geomorphological Analysis of the Vityaz and Vanuatu Trenches, Fiji Basin*. Geodetski List, 74(97), 1, 19–39.
17. Lemenkova, P. (2020b). *Visualization of the geophysical settings in the Philippine Sea margins by means of GMT and ISC data*. Central European Journal of Geography and Sustainable Development, *2*(1), 5–15.
18. Lemenkova P., (2019a), *Geomorphological modelling and mapping of the Peru-Chile Trench by GMT*. Polish Cartographical Review 51(4), 181–194.
19. Lemenkova P., (2019b), *Topographic surface modelling using raster grid datasets by GMT: example of the Kuril-Kamchatka Trench, Pacific Ocean*. Reports on Geodesy and Geoinformatics, 108, 9–22.
20. Lemenkova P., (2019c), *GMT Based Comparative Analysis and Geomorphological Mapping of the Kermadec and Tonga Trenches, Southwest Pacific Ocean*. Geographia Technica, 14(2), 39–48.
21. Lemenkova P., (2019d), *Geophysical Modelling of the Middle America Trench using GMT*. Annals of Valahia University of Targoviste. Geographical Series, 19(2), 73–94.
22. Lemenkova P., (2019e), *Automatic Data Processing for Visualising Yap and Palau Trenches by Generic Mapping Tools.* Cartographic Letters 27(2), 72–89.
23. Lemenkova P., (2019f), *Statistical Analysis of the Mariana Trench Geomorphology Using R Programming Language*. Geodesy and Cartography, 45(2), 57–84.
24. Lemenkova P., (2019g), *AWK and GNU Octave Programming Languages Integrated with Generic Mapping Tools for Geomorphological Analysis.* GeoScience Engineering, 65 (4), 1–22.
25. Lemenkova P., (2018), *R scripting libraries for comparative analysis of the correlation methods to identify factors affecting Mariana Trench formation*. Journal of Marine Technology and Environment, 2, 35–42.

26. Lemenkova P., (2011), *Seagrass Mapping and Monitoring Along the Coasts of Crete, Greece.* M.Sc. Thesis. Netherlands: University of Twente.
27. Lemoine F.G., Kenyon S.C., Factor J.K., et al. (1998), *NASA/TP-1998-206861: The Development of the Joint NASA GSFC and NIMA Geopotential Model EGM96*, NASA Goddard Space Flight Center, Greenbelt, Maryland, 20771 USA.
28. Leontiev O.K., Udintseva O.G., (1971), *The area of the main morphostructural elements of the ocean floor*. Bulletin of Moscow State University. Series 4, Geology, 2, 47-51.
29. Litvin V.M., (1987), *Morphostructure of the ocean seafloor*. Nedra, Leningrad.
30. Macdonald K.C., (1982), *Mid-Ocean Ridges: Fine Scale Tectonic, Volcanic and Hydrothermal Processes Within the Plate Boundary Zone*. Annual Review of Earth and Planetary Sciences. 10(1), 155–190.
31. Macdonald K.C., (2019), *Mid-Ocean Ridge Tectonics, Volcanism, and Geomorphology*. Encyclopedia of Ocean Sciences, 4, 405–419.
32. Matthews K.J., Müller R.D., Wessel P., Whittaker J.M., (2011), *The tectonic fabric of the ocean basins*, Journal of Geophysical Research, 116 (B12).
33. Müller R.D., Sdrolias M., Gaina C., Roest, W.R., (2008), *Age, spreading rates, and spreading asymmetry of the world's ocean crust*. Geochemistry, Geophysics, Geosystems, 9 (4), Q04006.
34. Paulatto M., Canales J.P., Dunn R.A., Sohn R.A., (2015), *Heterogeneous and asymmetric crustal accretion: New constraints from multibeam bathymetry and potential field data from the Rainbow area of the Mid-Atlantic Ridge (36815'N).* Geochemistry, Geophysics, Geosystems, 16, 2994–3014.
35. Sandwell D.T., Müller R.D., Smith W.H.F., Garcia E., Francis R., (2014), *New global marine gravity model from CryoSat-2 and Jason-1 reveals buried tectonic structure*. Science, 346 (6205), 65–67.
36. Schenke H.W., Lemenkova, P., (2008), *Zur Frage der Meeresboden-Kartographie: Die Nutzung von AutoTrace Digitizer für die Vektorisierung der Bathymetrischen Daten in der Petschora-See*. Hydrographische Nachrichten, 81, 16–21.
37. Seton M., Whittaker J., Wessel P., Müller R.D., DeMets C., Merkouriev S., Cande S., et al. (2014), *Community infrastructure and repository for marine magnetic identifications*. Geochemistry, Geophysics, Geosystems, 5(4), 1629-1641.
38. Smith W.H.F., Sandwell D.T., (1995), *Marine gravity field from declassified Geosat and ERS-1 altimetry*. EOS Transactions AGU, 76, F156.
39. Straume E.O., Gaina C., Medvedev S., Hochmuth K., Gohl K., Whittaker J.M., et al. (2019), *GlobSed: Updated total sediment thickness in the world's oceans*. Geochemistry, Geophysics, Geosystems, 20.
40. Suetova I.A., Ushakova L.A., Lemenkova P., (2005a), *Geoinformation mapping of the Barents and Pechora Seas*. Geography and Natural Resources, 4, 138–142.
41. Suetova, I.A., Ushakova, L.A., Lemenkova, P., (2005b), Geoecological Mapping of the Barents Sea Using GIS. International Cartographic Conference (ICC), July 9–16, 2005. La Coruna, Spain.
42. Udintsev G.B., (1959), *Studies of the bottom topography of the seas and oceans*. Itogi nauki. Dostizhenija okeanologii, 1, 27–90.

43. Udintsev G.B., (1989), *Regional geomorphology of the bottom of the oceans*. Indian Ocean. Science, Moscow.
44. Weissel J.K., Hayes D.E., (1971), *Asymmetric Seafloor Spreading south of Australia*. Nature, 231 (5304), 518–522.
45. Wessel P., Smith W.H.F., Scharroo R., Luis J.F., Wobbe F., (2013), *Generic mapping tools: improved version released*. EOS Transactions American Geophysical Union, 94(45), 409–410.
46. Wessel P., Smith W.H.F., (2018), T*he generic mapping tools. Version 4.5.18 Technical reference and cookbook (Computer software manual)*. U.S.A.
47. Wessel P., Smith W.H.F., Scharroo R., Luis J., Wobbe F., (2019), *The generic mapping tools. GMT man pages*. Release 5.4.5 (Computer software manual). U.S.A.